Lithuanian Journal of Physics
Vol. **64**, No. 3, pp. 177–188 (2024)
ISSN 1648-8504 eISSN 2424-3647
DOI: https://doi.org/10.3952/physics.2024.64.3.3

EFFECT OF $CaCO_3$, $SrCO_3$ AND $BaCO_3$ ADDITIONS ON THE MICROSTRUCTURE AND ELECTRICAL CHARACTERISTICS OF SnO_2-BASED VARISTOR CERAMICS

A. Gaponov

Oles Honchar Dnipro National University, 72 Gagarin Avenue, 49010 Dnipro, Ukraine
Email: alexei_gaponov@ukr.net

Received 18 December 2023; revised 2 May 2024; accepted 25 May 2024

The ceramic varistors SnO_2–Co_3O_4–Nb_2O_5–Cr_2O_3 with the addition of $CaCO_3$, $SrCO_3$ or $BaCO_3$ were sintered at temperatures 1250 and 1350°C, then their structures and electrical properties were studied. In all samples, the SnO_2 cassiterite phase with a rutile-type structure and the Co_2SnO_4 phase with a spinel-type structure were observed. All materials exhibited a highly nonlinear dependence of the current density on the electric field with the nonlinearity coefficient 24–50. When alkaline earth metal carbonates were added, the grain size of all samples decreased and the electric field E_1 increased. The addition of $CaCO_3$ lead to the decrease of the low-field electrical conductivity of varistors. The lowest low-field conductivities $4{\cdot}10^{-13}$ and $6{\cdot}10^{-13}$ Ω^{-1} cm^{-1} were found in the samples with $CaCO_3$ addition baked at 1250 and 1350°C, respectively. The observed effect is due to the increase of the potential barrier height at the SnO_2 grain boundaries by 7 and 13%, respectively, and the decrease of the grain size by 26 and 28% compared to SnO_2-based varistor ceramics without $CaCO_3$ addition.

Keywords: electrical conductivity, alkaline earth metal carbonates, tin oxide, varistor, ceramics

PACS: 73.30.+y, 73.40.Ty, 73.50.Fq

1. Introduction

Tin oxide is widely used for the production of gas sensitive sensors, varistors, piezoelectric devices, etc. [1–3]. Varistors are used as protecting devices against voltage transients in electrotechnical equipment. ZnO-based ceramic varistors [2, 3] and their alternative SnO_2-based ceramic varistors have been studied in some papers, for example, Refs. [2–12]. The properties of SnO_2-based varistors are similar to the ones observed in ZnO-based varistors [2, 3]. Tin oxide based varistor ceramics has high nonlinear current–voltage characteristics, for example, in the SnO_2–CoO (or Co_2O_3, Co_3O_4)–Nb_2O_5–Cr_2O_3 (SnCoNbCr) system [4–12].

Different oxides modify the microstructure and change the electrical characteristics of varistor ceramics. Cobalt oxides are usually used to improve the densification of ceramics [4, 13]. Cobalt oxides formed the solid solutions in SnO_2 and oxygen vacancies. They controlled the process of diffusion according to the reaction represented by the Kroger–Vink notation:

$$CoO \xrightarrow{SnO_2} Co''_{Sn} + V_O^{\bullet\bullet} + O_O^x, \quad (1)$$

$$Co_2O_3 \xrightarrow{SnO_2} 2Co'_{Sn} + V_O^{\bullet\bullet} + 2O_O^x + \frac{1}{2}O_2 \uparrow. \quad (2)$$

Niobium oxide Nb_2O_5 increases the electrical conductivity of SnO_2 grains due to the substitution of Sn^{4+} by Nb^{5+} [5, 14]. This effect can be described by the following equation:

$$Nb_2O_5 \xrightarrow{SnO_2} 2Nb_{Sn}^{\bullet} + 2e' + 4O_O^x + \frac{1}{2}O_2 \uparrow. \quad (3)$$

Chromium oxide Cr_2O_3 is often applied in order to improve the nonlinear current–voltage characteristics and the homogeneity of the material structure [6, 15]. This addition increases the height of potential barriers at the SnO_2 grain boundaries due

to the formation of oxygen vacancies. It can be represented by the following reaction:

$$Cr_2O_3 \xrightarrow{SnO_2} 2Cr'_{Sn} + V_O^{\bullet\bullet} + 2O_O^x + \frac{1}{2}O_2 \uparrow . \quad (4)$$

However, the low-field electrical conductivity $\sigma = 10^{-11}$–10^{-9} Ω^{-1} cm^{-1} [6, 8] and the leakage current density j_L = 0.2–70 μA cm^{-2} [5, 7, 10–12] are relatively high in SnCoNbCr varistors with different additions. Probably, such large values of these obtained parameters can be explained by a low quantity of intergranular phases in this ceramics. Meanwhile, for varistor application the low-field electrical conductivity and leakage current density should be relatively low. For the best ceramic varistors they could be nearly 10^{-13}–10^{-12} Ω^{-1} cm^{-1} and 0.01–0.1 μA cm^{-2}, respectively. To decrease the electrical conductivity at the low field and leakage current in the SnCoNbCr varistor some specific additions, in particular those with a large ionic radius, could be used [9]. They are the carbonates of alkaline earth metals Ca, Sr and Ba. The oxides of alkaline earth metals Ca, Sr and Ba interact with water in the process of ceramics preparation with the formation of sparingly soluble hydroxides. Therefore, in this paper we described the use of carbonates $CaCO_3$, $SrCO_3$ and $BaCO_3$ as additions for SnO_2-based ceramics.

The influence of $BaCO_3$ (0, 0.1, 0.25, 0.5 and 1.0 mol.%) and $SrCO_3$ (0, 1.5, 2.0 and 2.5 mol.%) additions on the electrical properties of the SnO_2 – 0.75 Co_2O_3 – 0.1 Ta_2O_5 varistor system has been studied earlier in papers [16] and [17], respectively. The highest nonlinearity coefficient α = 29.2 was obtained in the samples with 1.0 mol.% $BaCO_3$ [16] and α = 24.0 in the samples with 2.0 mol.% $SrCO_3$ [17]. But these samples have the highest electric field E_1 (at current density 1 mA cm^{-2}) – 28345 and 22040 V cm^{-1}, respectively. The samples without $BaCO_3$ or $SrCO_3$ additions have the lowest values of E_1 = 3780 and 3180 V cm^{-1}, respectively, while their nonlinearity coefficients α are not too high (12.6 [16] and 20.1 [17]).

The influence of $BaCO_3$ and $SrCO_3$ additions (0.5 and 1.0 at.%) on the electrical properties of the SnO_2 – 1.0 CoO – 0.5 Ta_2O_5 system has been investigated in paper [18]. The highest nonlinearity coefficient 52 was received in the sample with 0.5 at.% $BaCO_3$ and α = 36 in the sample with 1.0 at.% $SrCO_3$. But these samples do not have too high electric field, E_1 = 5025 and 5035 V cm^{-1}, respectively, and they do not differ too much from the value of E_1 = 4910 V cm^{-1} which was obtained in ceramics without alkaline earth metal carbonates [18].

In order to increase the electrical conductivity of ceramic grains the Nb_2O_5 and Sb_2O_5 additions were used instead of Ta_2O_5. The effect of $SrCO_3$ (0, 0.25, 0.5, 0.75 and 1.5 mol.%) on the microstructure and electrical properties of SnO_2 – 0.75 Co_2O_3 – 0.1 Nb_2O_5 ceramics and that of $CaCO_3$ (0, 0.1, 0.5 and 1.0 mol.%) on SnO_2 – 1.0 Co_3O_4 – 0.05 Sb_2O_5 ceramics were considered in papers [19] and [20], respectively. The highest nonlinearity coefficients 24.9 and 12.9 were obtained in the samples with 0.5 mol.% $SrCO_3$ and 0.1 mol.% $CaCO_3$, respectively. But we consider that these values were not high enough at breakdown electric fields E_1 = 3695 V cm^{-1} [19] and E_1 = 376 V cm^{-1} [20]. The values of nonlinearity coefficient decreased down to 13.1 at E_1 = 2606 V cm^{-1} [19] or 10.6 at E_1 = 378 V cm^{-1} [20] when the $SrCO_3$ or $CaCO_3$ additions were not used.

The microstructure and electrical properties of SnO_2 – 5.0 Co_3O_4 – 0.4 Sb_2O_5 ceramic varistors with additions of 0.4 mol.% $CaCO_3$, $SrCO_3$ or $BaCO_3$ were investigated in paper [21]. The highest nonlinearity coefficient α = 5.0 (it should be noted that it is quite a small value) was obtained in the sample with $CaCO_3$ addition. This value α = 5.0 did not correspond with the lowest value of voltage for one barrier V_b = 0.20 V·b^{-1} (at $SrCO_3$ addition α = 2.7 and V_b = 0.35 V·b^{-1}, at $BaCO_3$ addition α = 4.9 and V_b = 0.61 V·b^{-1} [21]). Such contradiction is not explained in paper [21]. Besides, the quite large values of electrical conductivity of such ceramics $\sigma = 1{\cdot}10^{-8} - 4{\cdot}10^{-7}$ Ω^{-1} cm^{-1} show that the leakage current of such varistors is too high. The $CaCO_3$ or $SrCO_3$ additions lead even to some increase of σ values [21]. Therefore, such ceramics can hardly be used for varistor manufacture.

The non-ohmic properties of the SnO_2 – 0.5 Co_3O_4 – 0.05 Cr_2O_3 – 0.05 Nb_2O_5 ceramic system with 0.5 mol.% $CaCO_3$, $SrCO_3$ or $BaCO_3$ additions were studied in paper [22]. The nonlinearity coefficient α = 2.6–10.0 and the potential barrier height at the SnO_2 grain boundaries

φ = 0.46–0.57 eV in these samples are rather small values for SnO_2-based varistors. Besides, such ceramics have rather large values of electrical conductivity $\sigma = 2{\cdot}10^{-5}$–$5{\cdot}10^{-5}$ Ω^{-1} cm^{-1} [22].

However, in our obtained SnO_2 – 0.5 Co_3O_4 – 0.05 Nb_2O_5 – 0.05 Cr_2O_3 – 0.5 CuO system [9] the additions of 0.5 mol.% $CaCO_3$ or $BaCO_3$ lead to the decrease of the low-field electrical conductivity of ceramics. The varistors with $CaCO_3$ addition have the high nonlinear current–voltage characteristics and the highest value of nonlinearity coefficient α = 58 at E_1 = 2960 V cm^{-1} [9]. However, the presence of CuO addition caused rather high values of the low-field electrical conductivity of samples [9]. Therefore, it is useful to bake the SnCoNbCr ceramics without CuO but with $CaCO_3$, $SrCO_3$ or $BaCO_3$ additions at different temperatures, which may result in obtaining higher values of the nonlinearity coefficient α and lower values of the low-field electrical conductivity σ. It is also necessary to investigate the properties of the samples obtained at different bake temperatures and compare their electrical characteristics.

Hence the purpose of our paper is to study in detail the influence of carbonates of alkaline earth metals (Ca, Sr and Ba) on the microstructure and electrical properties of SnCoNbCr system. We pay special attention to the increase of the nonlinearity of current–voltage characteristics and the decrease of the low-field electrical conductivity of SnO_2-based varistor ceramics.

2. Experimental details

The samples (99.4-x) SnO_2 – 0.5 Co_3O_4 – 0.05 Nb_2O_5 – 0.05 Cr_2O_3 – x $MeCO_3$ (mol.%, x = 0 or 0.5; *Me* = Ca, Sr, Ba) were prepared by a conventional mixture method. The mixture of powders was wet-milled with distilled water and pressed in discs 12 mm in diameter and about 0.8 mm thick under axial pressure 45 MPa. The pressed discs were sintered in air at the temperatures 1250 and 1350°C and slowly cooled to room temperature. The baking temperatures lower than 1250°C worsen the sintering of samples, but the baking temperatures higher than 1350°C lead to the decrease of nonlinear current–voltage characteristics of ceramics [23]. In-Ga-eutectic electrodes were used in the tested varistors.

The shrinkage γ was calculated according to the expression $\gamma = (D_0 - D)/D_0$, where D_0 and D are the diameters of the sample before and after sintering, respectively. The density of samples ρ was estimated with the help of the Archimedes method using the analytical scales ADV-200 (a weighing accuracy of 0.1 mg).

The microstructure of ceramics was studied by a scanning electron microscope (SEM) Zeiss Supra 35VP. Average grain sizes l_g were calculated by the equation $l_g = 1.558\,L/n$, in which n is the number of grains intercepted by a test line with the known length L (μm) [24]. The phase identification of as-prepared samples was determined by the X-ray diffraction technique (XRD) using a DRON-2.0 diffractometer equipment with a $Co_{K\alpha}$ radiation source (λ = 1.7903 Å) and a setting of 40 kV, 14 mA and 1°/min. In order to detect possible phase transitions and mass change, differential thermal analysis and thermo-gravimetry were performed in the range 20–1350°C with the heating rate 7.5°C/min using the F. Paulik, J. Paulik, L. Erdey system derivatograph manufactured by MOM.

The current–voltage characteristics at DC voltage and the steady-state current were measured. The possible self-heating of the samples during the measurement was detected as the increase of current at a fixed voltage. The results were obtained avoiding the self-heating of samples.

The nonlinearity coefficient $\alpha = \log (j_1/j_{0.1})/\log (E_1/E_{0.1})$ was estimated as the slope of current–voltage characteristic plotted in the double logarithmic scale $\log j - \log E$. The values of electric field E_1 and $E_{0.1}$ were obtained at the current density j_1 = 1 mA cm^{-2} and $j_{0.1}$ = 0.1 mA cm^{-2}. The leakage current density j_L was measured at 0.75 E_1. The number of grain boundaries between the electrodes of ceramics N_b was determined as t/l_g, where t is the thickness of sample and l_g is the average grain size.

The activation energy of electrical conduction E_σ is found from the temperature dependence of electrical conductivity σ according to the expression $\sigma(T) = \sigma_0 \exp(-E_\sigma/kT)$, where k is the Boltzmann constant and T is the absolute temperature.

The dielectric permittivity of the ceramics was calculated with the formula $\varepsilon = Ct/(\varepsilon_0 S)$, where t is the sample thickness, S is the electrode area, and ε_0 is the electric constant. The capacitance C at 1 kHz was measured by a *LCRG* device Tesla BM 591.

3. Results and discussion

3.1. Microstructure and phase composition

The micrographs of studied ceramics are represented in Fig. 1. They show that in all samples the SnO_2 grains and small crystal-like inclusions are seen. The measured average SnO_2 grain size l_g in the SnCoNbCr ceramics sintered at 1250°C was 3.5 μm. The additions of the carbonates of alkaline earth metals Ca, Sr or Ba lead to the decrease of the value l_g to 2.6, 1.3 or 0.8 μm, respectively (Table 1). At the increase of sintered temperatures up to 1350°C, the grains grow intensively and the average SnO_2 grain size is larger (see Table 2). But the values l_g decrease at the addition of carbonates Ca, Sr or Ba from 6.8 to 4.7 μm. The reason is that the ionic radii of Ca^{2+} (104 pm), Sr^{2+} (120 pm) and Ba^{2+} (138 pm) are larger than that of Sn^{4+} (67 pm). The positively charged ions tend to be incorporated into the SnO_2 systems and modify the microstructure of samples [9]. They can be segregated at the grain boundaries limiting the grain coarsening. Then the bigger the ionic radius of the element is, the smaller the growth of grains is. Therefore, the average SnO_2 grain size decreases at sintering of the samples with $CaCO_3$, $SrCO_3$ or $BaCO_3$ additions (Tables 1 and 2).

In Fig. 1, one can see that small crystal-like inclusions appear in the area of large tin-oxide grains (marked by letters A). In order to find out their composition, the X-ray phase diffraction analysis of all samples was carried out. The representative XRD analysis of all research materials is shown in Fig. 2. The identified peaks in all samples correspond to the SnO_2 cassiterite phase with a rutile-type structure (ICDD PDF # 00-041-1445, here ICDD stands for International Centre for Diffraction Data, Newtown Square, PA). The sample with the addition of $BaCO_3$ has both small crystallites and rather large SnO_2 grains (see Fig. 1(d)). The XRD signal from large

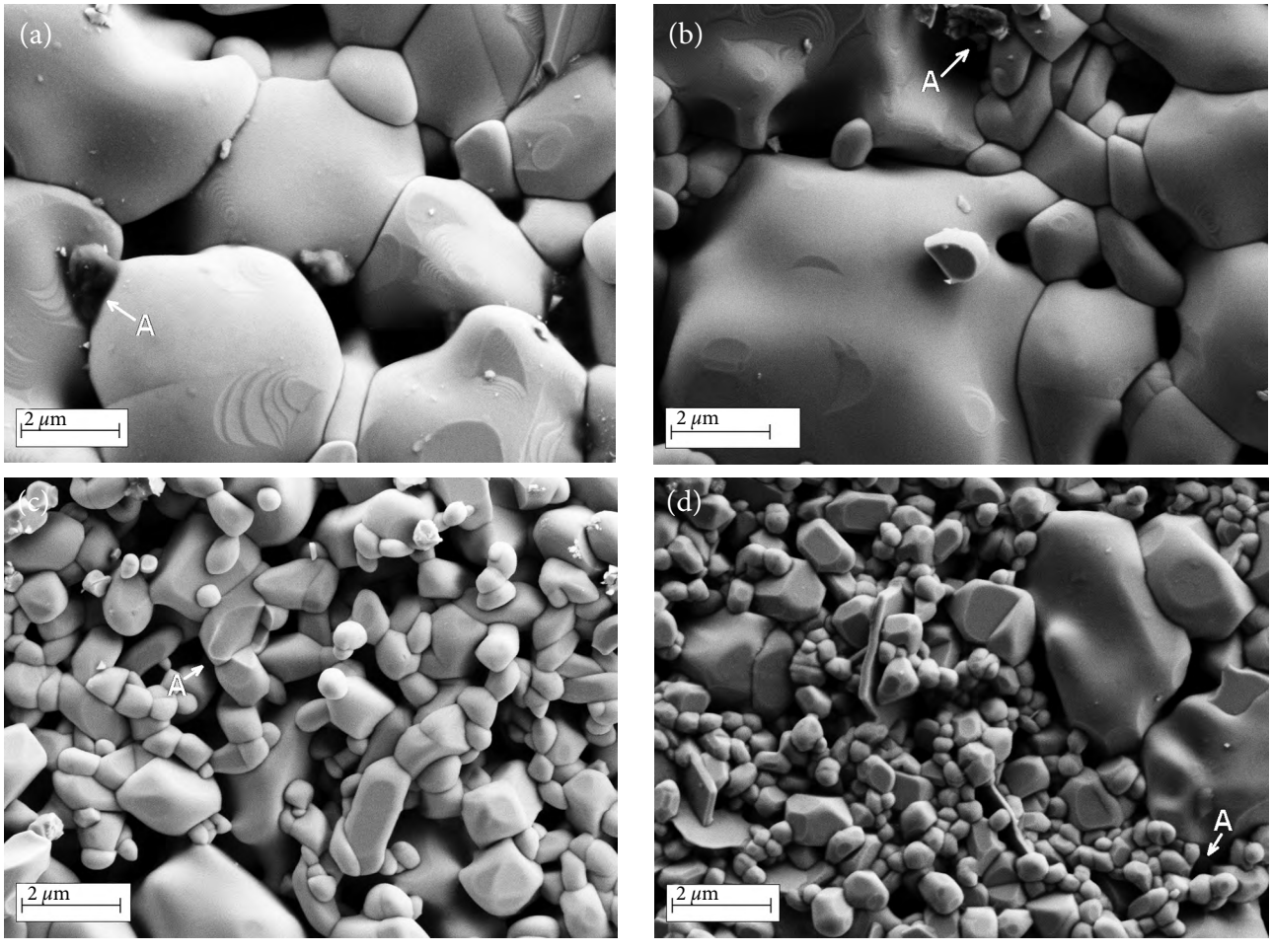

Fig. 1. SEM micrographs of the fractured surface of SnO_2–Co_3O_4–Nb_2O_5–Cr_2O_3 ceramics (a) and the samples with $CaCO_3$ (b), $SrCO_3$ (c) or $BaCO_3$ (d) additions sintered at 1250°C.

Table 1. Parameters of tin dioxide based non-ohmic ceramics (sintered at 1250°C). The relative changes of physical parameter values in percent are given as subscripts.

Ceramic system	SnCoNbCr	SnCoNbCrCa	SnCoNbCrSr	SnCoNbCrBa
Average grain size l_g, μm	3.5	2.6 $_{-25.7\%}$	1.3 $_{-62.9\%}$	0.8 $_{-77.1\%}$
Linear shrinkage γ, %	8.3	6.3 $_{-24.1\%}$	3.6 $_{-56.6\%}$	7.3 $_{-12.0\%}$
Density ρ, g/cm^3	6.51	6.48 $_{-0.5\%}$	6.44 $_{-1.1\%}$	6.49 $_{-0.3\%}$
Number of grain boundaries N_b	194	335 $_{+72.7\%}$	731 $_{+276.8\%}$	988 $_{+409.3\%}$
Nonlinearity coefficient α	49	30 $_{-38.8\%}$	24 $_{-51.0\%}$	40 $_{-18.4\%}$
Electric field E_1, V cm^{-1}	5650	7040 $_{+24.6\%}$	11250 $_{+99.1\%}$	7710 $_{+36.5\%}$
Activation energy of electrical conduction E_σ, eV	1.00	1.07 $_{+7.0\%}$	1.17 $_{+17.0\%}$	0.93 $_{-7.0\%}$
Low-field electrical conductivity σ, Ω^{-1} cm^{-1}	$0.9\cdot10^{-12}$	$0.4\cdot10^{-12}$ $_{-55.6\%}$	$1.8\cdot10^{-12}$ $_{+100.0\%}$	$2\cdot10^{-12}$ $_{+122.2\%}$
Leakage current density j_L, μA cm^{-2}	0.11	0.19 $_{+72.7\%}$	1.53 $_{+1291.9\%}$	0.14 $_{+27.3\%}$
Dielectric permittivity ε	274	78 $_{-71.5\%}$	28 $_{-89.8\%}$	149 $_{-45.6\%}$

Table 2. Parameters of tin dioxide based non-ohmic ceramics (sintered at 1350°C). The relative changes of physical parameter values in percent are given as subscripts.

Ceramic system	SnCoNbCr	SnCoNbCrCa	SnCoNbCrSr	SnCoNbCrBa
Average grain size l_g, μm	6.8	4.9 $_{-27.9\%}$	4.8 $_{-29.4\%}$	4.7 $_{-30.9\%}$
Linear shrinkage γ, %	9.2	7.8 $_{-15.2\%}$	5.6 $_{-39.1\%}$	8.3 $_{-9.8\%}$
Density ρ, g/cm^3	6.79	6.62 $_{-2.5\%}$	6.49 $_{-4.4\%}$	6.71 $_{-1.2\%}$
Number of grain boundaries N_b	96	110 $_{+14.6\%}$	160 $_{+66.7\%}$	151 $_{+57.3\%}$
Nonlinearity coefficient α	13	40 $_{+207.7\%}$	49 $_{+276.9\%}$	50 $_{+284.6\%}$
Electric field E_1, V cm^{-1}	3350	4520 $_{+34.9\%}$	5650 $_{+68.7\%}$	5890 $_{+75.8\%}$
Activation energy of electrical conduction E_σ, eV	0.90	1.02 $_{+13.3\%}$	0.93 $_{+3.3\%}$	0.86 $_{-4.4\%}$
Low-field electrical conductivity σ, Ω^{-1} cm^{-1}	$1.7\cdot10^{-12}$	$0.6\cdot10^{-12}$ $_{-64.7\%}$	$3.0\cdot10^{-12}$ $_{+76.5\%}$	$8.5\cdot10^{-12}$ $_{+400.0\%}$
Leakage current density j_L, μA cm^{-2}	7.94	0.03 $_{-99.6\%}$	0.06 $_{-99.2\%}$	0.49 $_{-93.8\%}$
Dielectric permittivity ε	626	229 $_{-63.4\%}$	127 $_{-79.7\%}$	305 $_{-51.3\%}$

SnO_2 grains probably gives more intense peaks compared to other samples. Additionally, some small peaks were also observed in all samples. These diffraction peaks correspond to the crystal planes of (311), (400), (331) and (422), they were indexed and it is matched with the standard Co_2SnO_4 phase with a spinel-type structure (ICDD PDF # 00-029-0514). More visible peaks of the Co_2SnO_4 phase were found in the ceramics with $SrCO_3$ or $BaCO_3$ additions (for example, see the insert on Fig. 2). It should be noted that other phases can exist in the samples, for example, $CoSnO_3$ which is mentioned in paper [25] or $CaSnO_3$ [20]. But the concentrations of Nb_2O_5, Cr_2O_3, $CaCO_3$, $SrCO_3$ and $BaCO_3$ additions were too small to be detected by an X-ray apparatus. Therefore, in our paper only the SnO_2 phase and the Co_2SnO_4 phase are observed. A low quantity of the Co_2SnO_4 intergranular phase in ceramics should be useful for the decrease of electrical conductivity of ceramics. This assumption needs to be proven later.

The absence of Co_3O_4 and the presence of Co_2SnO_4 phase in all samples are explained by the decomposition reaction. At the temperature between 900 and 960°C, the Co_3O_4 can decompose according to the following equation [13, 21]:

$$2Co_3O_4 \rightarrow 6CoO + O_2\uparrow. \quad (5)$$

Then the CoO reacts with the SnO_2 and the Co_2SnO_4 spinel phase is obtained according to the following reaction [21, 26]:

$$2CoO + SnO_2 \rightarrow Co_2SnO_4. \quad (6)$$

In order to detect the decomposition of Co_3O_4, possible phase transitions and mass changes,

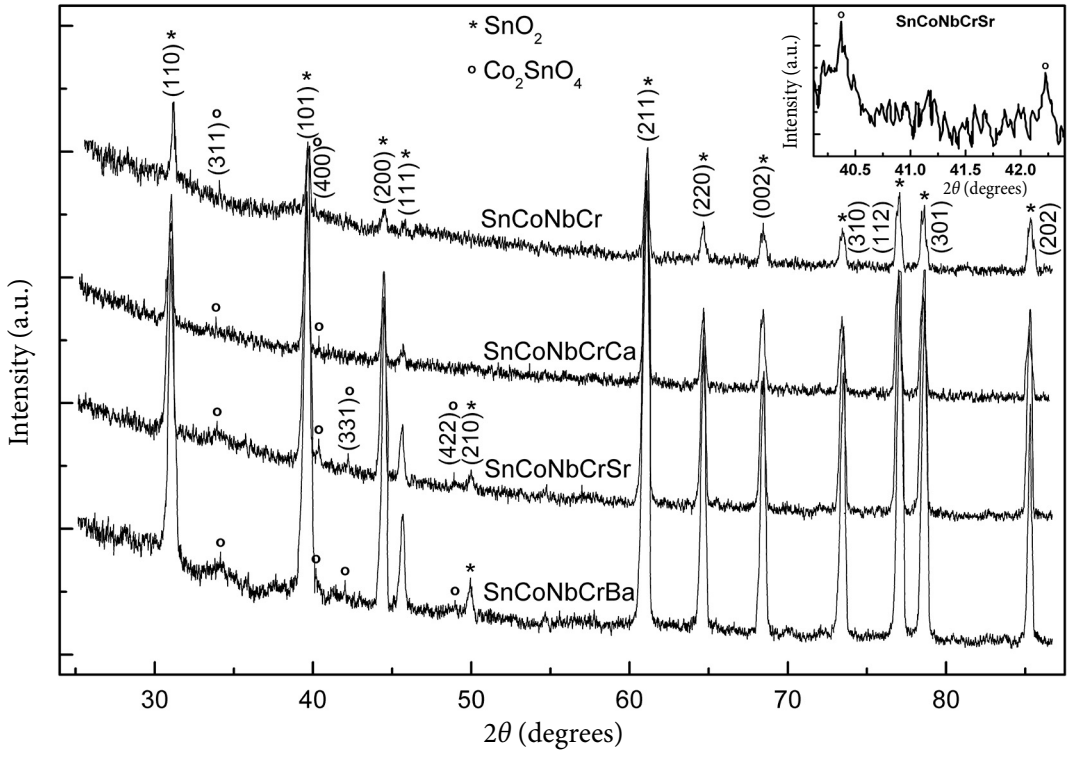

Fig. 2. XRD diagrams of the as-sintered surfaces of SnO_2–Co_3O_4–Nb_2O_5–Cr_2O_3 (SnCoNbCr) ceramics and the samples with $CaCO_3$ (SnCoNbCrCa), $SrCO_3$ (SnCoNbCrSr) or $BaCO_3$ (SnCoNbCrBa) additions (XRD diagram for the SnCoNbCrSr sample at $2\theta = 40.1 - 42.4°$ is shown in the insert).

the differential thermal (DTA) and thermo-gravimetrical (TGA) analyses of raw materials (without sintering) were performed. The DTA showed (Fig. 3(a)) that while heating all tested materials, slight endothermic peaks were observed at the temperature near 960°C. These peaks correspond to low weight losses in TGA (Fig. 3(b)). This situation is explained by the decomposition of Co_3O_4 into CoO according to Eq. (5). Then CoO reacts with SnO_2 and they generate the Co_2SnO_4 spinel phase according to Eq. (6).

Moreover, the TGA showed (Fig. 3(b)) the decrease of mass during heating mixtures with $CaCO_3$ (at 660–780°C), $SrCO_3$ (at 775–995°C) or $BaCO_3$ (at 780–1020°C) additions. It is caused by CO_2 emission during the decomposition of carbonates of alkaline earth metals and the transition of these substances into oxides CaO, SrO or BaO according to the following equation:

$$MeCo_3 \rightarrow MeO + CO_2\uparrow. \quad (7)$$

Here *Me* is Ca, Sr or Ba.

In order to receive additional information about the microstructure of ceramics, the linear shrinkage γ and the density ρ of all samples were measured (Tables 1 and 2). The values of linear shrinkage $\gamma = 8.3\%$ and the density $\rho = 6.51$ g/cm^3 for the SnCoNbCr sample sintered at the temperature 1250°C are lower than those for the sample sintered at 1350°C ($\gamma = 9.2\%$, $\rho = 6.79$ g/cm^3). With increasing the sintering temperature, the grains grow more intensively, they are located more solidly, and therefore the shrinkage and the density of samples are higher.

The $CaCO_3$, $SrCO_3$ or $BaCO_3$ additions to the SnCoNbCr system lead to lower values of linear shrinkages and the densities of samples: 6.3, 3.6, 7.3% and 6.49, 6.44, 6.46 g/cm^3 at baking temperature 1250°C (Table 1) and 7.8, 5.6, 8.3% and 6.62, 6.49, 6.71 g/cm^3 at baking temperature 1350°C, respectively (Table 2). The metal ions Me^{2+} with a larger ionic radius can be incorporated into the SnO_2 systems and the grains grow slower. Therefore, the linear shrinkage and the density values of the samples with addition of the carbonates of alkaline earth metals Ca, Sr and Ba are lower than those of SnCoNbCr samples.

The $CaCO_3$ addition to SnCoNbCr ceramics leads to the formation of both rather small and

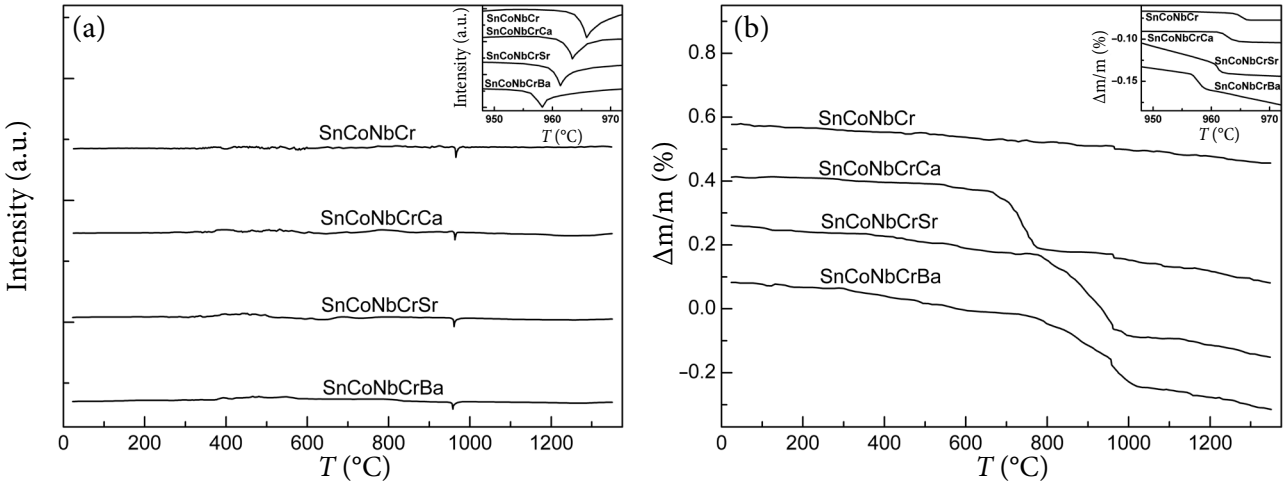

Fig. 3. DTA (a) and TGA (b) of the raw mixture of SnO_2–Co_3O_4–Nb_2O_5–Cr_2O_3 (SnCoNbCr) material and the mixtures with $CaCO_3$ (SnCoNbCrCa), $SrCO_3$ (SnCoNbCrSr) or $BaCO_3$ (SnCoNbCrBa) additions (DTA and TGA for all mixtures at temperatures 948–972°C are shown in the inserts).

very large grains (Fig. 1(b)). They are located less densely. So, the shrinkage and the density values of SnCoNbCrCa samples are lower than those of SnCoNbCr ceramics.

In case of $SrCO_3$ addition to the SnO_2-based ceramics, the Sr^{2+} ions with a bigger ionic radius (120 pm) formed Sr-rich phases which inhibited the SnO_2 grain growth. As a result, the grains of such ceramics grow slowly (Fig. 1(c)) and the material densification is less.

The Ba^{2+} ions with the biggest ionic radius (138 pm) can be segregated at the grain boundaries and that allows obtaining the grains with different forms and sizes (see Fig. 1(d)). They are located rather close to each other, and therefore the linear shrinkages and the densities of the samples with $BaCO_3$ addition are larger than those of the samples with $CaCO_3$ and $SrCO_3$ additions (Tables 1 and 2).

Thus, the results of the thermal analyses together with the microstructure characteristics obtained by SEM and XRD showed that reactions (5) and (6) had occurred at nearly 960°C and finally the spinel phase Co_2SnO_4 had been formed. The carbonates of alkaline earth metals Ca, Sr and Ba decomposed at heating and turned into oxides CaO, SrO and BaO, respectively.

3.2. Electrical properties

Current–voltage characteristics of the samples were measured for the ceramics obtained at sintered temperatures 1250 and 1350°C. They are represented at the coordinate of log j – log E as shown in Fig. 4. The electrical parameters of these materials are presented in Tables 1 and 2.

The current–voltage characteristic of the SnCoNbCr sample obtained at 1250°C is highly nonlinear (Fig. 4(a), curve 1). The addition of alkaline earth metal carbonates leads to a slight decrease of the nonlinear current–voltage characteristics (Fig. 4(a), curves 2–4), though the values of nonlinearity coefficient α remain quite high (Table 1). A rather large value $\alpha \approx 40$ is observed in the sample with $BaCO_3$ addition.

When carbonates of $CaCO_3$, $SrCO_3$ and $BaCO_3$ are added, a slight increase of the electric field E_1 is seen (Fig. 4(a), curves 2–4). The addition of $SrCO_3$ caused the highest value of electric field E_1 = 11250 V cm^{-1}. This value corresponds to the lower value of average grain size l_g = 1.3 μm and the lowest values of linear shrinkage γ = 3.6 % and density ρ = 6.44 g/cm^3 (Table 1). The additions of alkaline earth metal carbonates lead to the decrease of the grain size l_g and to the increase of the number of grain boundaries between electrodes N_b (Table 1). Therefore, the values of electric field E_1 became larger. The same changes are also observed at baking temperature 1350°C (Fig. 4(b)). The decrease of the grain size in such ceramics from 6.8 to 4.7 μm (Table 2) leads to the increase of the electric field E_1 from 3350 to 5890 V cm^{-1}.

The rise of baking temperature from 1250 to 1350°C causes the growth of SnO_2 grains in the samples with corresponding additions (Tables 1

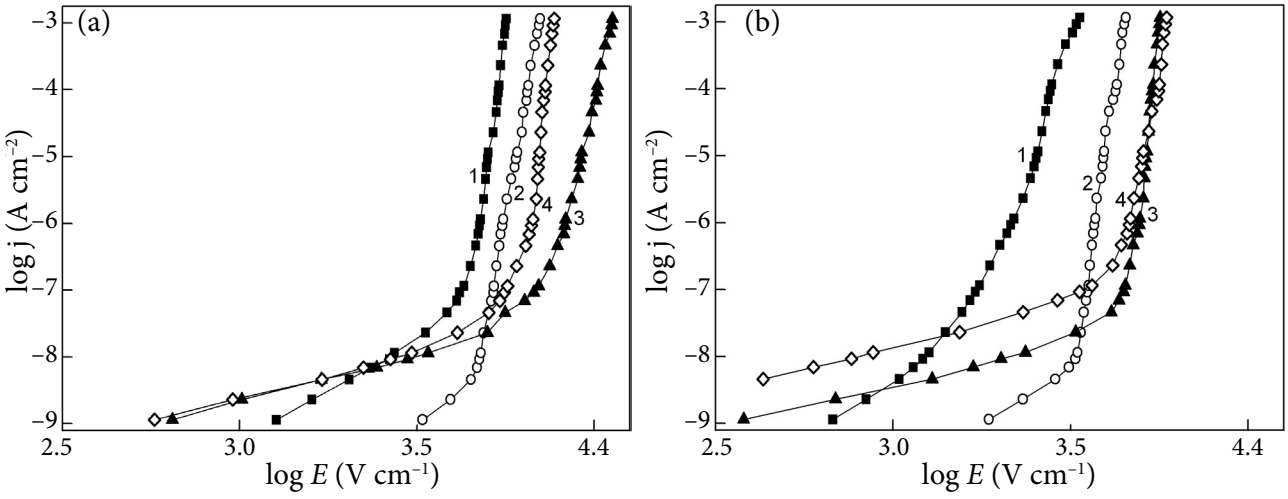

Fig. 4. Current density versus electric field for the SnO_2 – Co_3O_4 – Nb_2O_5 – Cr_2O_3 ceramics (1) and the samples with $CaCO_3$ (2), $SrCO_3$ (3) or $BaCO_3$ (4) additions sintered at 1250°C (a) and 1350°C (b).

and 2). Thus, the number of grains diminishes per unit length. The number of grain boundaries N_b and, respectevly, voltage barriers on the grain boundary also reduces (Tables 1 and 2). Therefore, the electric field E_1 of the corresponding samples decreases at the raising of baking temperature and the relative dielectric permittivity ε increases (Tables 1 and 2), as it was reported earlier for SnO_2-based varistors in papers [9, 23].

A highly nonlinear part of the current–voltage characteristic of SnCoNbCr ceramics begins at the current density of about $1{\cdot}10^{-6}$ A cm^{-2} (Fig. 4(a), curve 1). This material has a relatively high low-field electrical conductivity. A larger decrease of low-field conductivity is observed in the case of $CaCO_3$ addition (Fig. 4(a), curve 2). The effect with a lower low-field conductivity also takes place at baking temperature 1350°C (Fig. 4(b)).

The decrease of low-field conductivity up to $4{\cdot}10^{-13}$ and $6{\cdot}10^{-13}$ Ohm$^{-1}{\cdot}$cm^{-1} in the samples with $CaCO_3$ addition (Tables 1 and 2) is related to the decrease of the grain size (a significant decrease of the grain-boundary cross-section, the increase of grain neck resistivity) and to the increase of the height of the potential barriers of grain boundaries (see below). The samples with $CaCO_3$ addition have the lower values of leakage current density j_L = 0.19 and 0.03 μA cm^{-2} (Tables 1 and 2). These values are quite low among the well-known ones [6, 7, 26–29].

To explain the observed decrease of the low-field conductivity in the samples with $CaCO_3$ addition, the temperature dependence of electrical conductivity σ was studied (Fig. 5). The equation $\sigma = \sigma_0 \exp(-E_\sigma/kT)$ is correct in the temperature range about 55–150°C (Fig. 5). The activation energy of electrical conduction E_σ gives an estimate of the potential barrier height φ at the SnO_2 grain boundaries because $E_\sigma = \varphi + \eta$ and $\eta << \varphi$ (here η is the distance between the conduction band edge and the Fermi level inside the grain) [30]. In the range about 30–55°C, the values of σ decrease at heating (Fig. 5) due to the desorption of water vapour [31, 32].

It is seen from Tables 1 and 2 that the values of E_σ slightly increase in the samples with $CaCO_3$ and $SrCO_3$ additions but decrease in the samples with $BaCO_3$ addition. At the same time, the low-field conductivity of samples decreases with $CaCO_3$ addition but increases with $SrCO_3$ and $BaCO_3$ additions (Tables 1 and 2).

The most probable reason of these processes in case of $CaCO_3$ addition is the increase of the grain-boundary resistance due to the decrease of the grain size l_g. The electrical conductivity σ of an idealized ceramic sample with equal grains and grain boundaries is proportional to the grain size, $\sigma \sim l_g$. The dielectric permittivity of an idealized ceramic material is also proportional to the grain size, $\varepsilon \sim l_g$ [31]. If in addition to the decrease of the grain size the barrier height at the grain boundaries increases, then the values σ and ε will decrease. This situation takes place in the samples with $CaCO_3$ addition (Tables 1 and 2). For such ceramics the average grain size l_g decreases by 26%

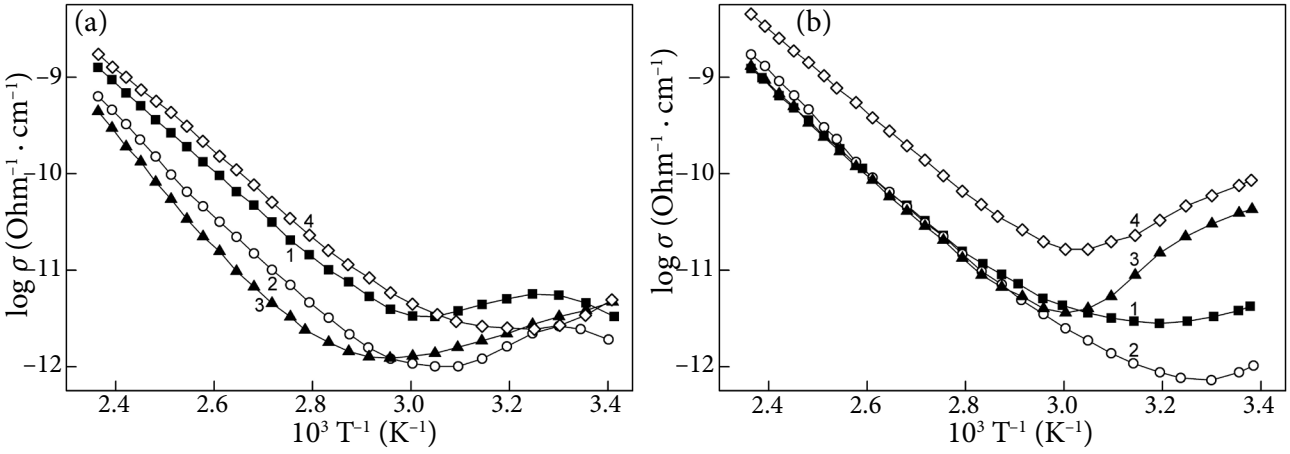

Fig. 5. Temperature dependence of electrical conductivity for the SnO_2–Co_3O_4–Nb_2O_5–Cr_2O_3 ceramics (1) and the samples with $CaCO_3$ (2), $SrCO_3$ (3) or $BaCO_3$ (4) additions sintered at 1250°C (a) and 1350°C (b).

for the sample baked at 1250°C and by 28% for the sample baked at 1350°C. The potential barrier height φ of varistors increases by 7% for the sample baked at 1250°C and by 13% for the sample baked at 1350°C. Therefore, the electrical conductivity σ of SnCoNbCrCa ceramics decreases by 56% for the sample baked at 1250°C and by 65% for the sample baked at 1350°C.

The decrease of values E_σ and therefore the lowering of the potential barrier height in the ceramics with $BaCO_3$ addition (Tables 1 and 2) explain the increase of the electrical conductivity σ of SnCoNbCrBa samples. However, the increase of the activation energy E_σ in the case of $SrCO_3$ addition (Tables 1 and 2) cannot explain the observed increase of electrical conductivity in SnCoNbCrSr ceramics (Fig. 4(a) and Fig. 4(b)). Therefore, other factors should be taken into account. The samples with $SrCO_3$ addition have quite small grains (l_g = 1.3 and 4.8 μm) and the lowest density (ρ = 6.44 and 6.49 g/cm^3), and they are rather porous (Fig. 1(c)). So, the humid air can achieve the grain boundaries and increase the electrical conductivity greatly. That assumption was verified experimentally by placing the samples in air at 10% relative humidity. In these conditions, the electrical conductivity of SnCoNbCrSr samples is close to that of SnCoNbCr samples.

Additionally, it was observed that DC conductivity, AC conductivity and capacitance of all samples decrease after the application of voltage (for example, after measuring the current–voltage characteristics), and then they are slowly restored to their initial values. The same situation also takes place at measuring the temperature dependence of electrical conductivity. This effect is similar to the one observed in ZnO varistors earlier [33]. It can be explained by the assumption that an application of voltage causes the additional filling of interface states by electrons. Due to the conservation of the electroneutrality, the depleted regions widen and the barrier height φ increases, and, respectively, capacitance, DC and AC conductivity of a sample decrease. After the elimination of applied voltage the captured electrons are emitted out of the interface states and the equilibrium is restored.

4. Conclusions

In SnO_2 – Co_3O_4 – Nb_2O_5 – Cr_2O_3 ceramics with the addition of alkaline earth metal carbonates $CaCO_3$, $SrCO_3$ and $BaCO_3$, the SnO_2 cassiterite phase with a rutile-type structure and the Co_2SnO_4 phase with a spinel-type structure were observed. The obtained varistors are materials with highly nonlinear current–voltage characteristics and the values of nonlinearity coefficient in the range 24–50. The highest nonlinearity coefficient $\alpha \approx 50$ is observed in the sample with $BaCO_3$ addition. All additions lead to the increase of the electric field E_1 due to the decrease of the SnO_2 grain size of ceramics. The addition of $SrCO_3$ causes the highest electric field E_1 = 11250 V cm^{-1}. The addition of $CaCO_3$ helps to decrease the low-field electrical conductivity (down to $0.6 \cdot 10^{-12}$ Ω^{-1} cm^{-1}) and the leakage current density (down to 0.03 μA cm^{-2}) of tin oxide based varistor ceramics baked at 1350°C. The observed decrease of the low-field

electrical conductivity by 65% correlates with the experimentally found increase of the activation energy of electrical conduction by 13% and the decrease of the SnO_2 grain size by 28%. The obtained ceramics can be used for the manufacture of varistors with low values of leakage current.

Acknowledgements

The author is very grateful to Dr. A.B. Glot (Universidad Tecnológica de la Mixteca, México) and Dr. R. Bulpett (Experimental Techniques Centre, Brunel University, England) for their help with the scanning electron microscopy. The author is also grateful to Dr. K.V. Chasovsky (Dnipro National University, Ukraine) for his help with the X-ray diffraction analysis.

References

[1] W. Gopel and K.D. Schierbaum, SnO_2 sensors: current status and future prospects, Sens. Actuat. B **26–27**, 1–12 (1995), https://doi.org/10.1016/0925-4005(94)01546-t

[2] A.B. Glot, Yu.N. Proshkin, and A.M. Nadzhafzade, Electrical properties of tin dioxide and zinc oxide ceramics, in: *Ceramics Today – Tomorrow's Ceramics*, Materials science monographs, Vol. 66C, ed. P. Vincenzini (Elsevier, 1991) pp. 2171–2180.

[3] P.R. Bueno, J.A. Varela, and E. Longo, SnO_2, ZnO and related polycrystalline compound semiconductors: An overview and review on the voltage-dependent resistance (non-ohmic) feature, J. Eur. Ceram. Soc. **28**(3), 505–529 (2008), https://doi.org/10.1016/j.jeurceramsoc.2007.06.011

[4] S.A. Pianaro, P.R. Bueno, E. Longo, and J.A. Varela, A new SnO_2-based varistor system, J. Mater. Sci. Lett. **14**(10), 692–694 (1995), https://doi.org/10.1007/BF00253373

[5] Q.Y. Wei, J.L. He, and J. Hu, Dependence of residual voltage ratio behavior of SnO_2-based varistors on Nb_2O_5 addition, Sci. China Tech. Sci. **54**(6), 1415–1418 (2011), https://doi.org/10.1007/s11431-011-4375-3

[6] S.A. Pianaro, P.R. Bueno, E. Longo, and J.A. Varela, Microstructure and electric properties of a SnO_2 based varistor, Ceram. Int. **25**, 1–6 (1999), https://doi.org/10.1016/S0272-8842(97)00076-X

[7] G. Hu, J. Zhu, H. Yang, and F. Wang, Effect of CuO addition on the microstructure and electrical properties of SnO_2-based varistor, J. Mater. Sci. **24**, 2944–2949 (2013), https://doi.org/10.1007/s10854-013-1195-1

[8] A.B. Glot, R. Bulpett, A.I. Ivon, and P.M. Gallegos-Acevedo, Electrical properties of SnO_2 ceramics for low voltage varistors, Phys. B **457**, 108–112 (2015), https://doi.org/10.1016/j.physb.2014.09.026

[9] A.V. Gaponov, O.V. Vorobiov, and A.M. Vasyliev, Electrical parameters of SnO_2 based varistor ceramics with CaO and BaO additions, Phys. Chem. Solid State **17**(1), 81–87 (2016), https://doi.org/10.15330/pcss.17.1.81–87

[10] M. Maleki Shahraki, M. Golmohammad, I. Safaee, and M. Delshad Chermahini, The control of abnormal grain growth in low-voltage SnO_2 varistors by microseed addition, Ceram. Int. **44**(3), 3388–3393 (2018), https://doi.org/10.1016/j.ceramint.2017.11.129

[11] D. Liu, W. Wang, K. Cheng, Q. Xie, Y. Zhou, and H. Zhao, High voltage gradient and low leakage current SnO_2 varistor ceramics doped with Y_2O_3 and Nb_2O_5, Mater. Chem. Phys. **242**, 122526 (2020), https://doi.org/10.1016/j.matchemphys.2019.122526

[12] M. Abdollahi, M. Reza Nilforoushan, M. Maleki Shahraki, M. Delshad Chermahini, and M. Moradizadeh, The degradation behavior of high-voltage SnO_2 based varistors sintered at different temperatures, Ceram. Int. **46**(8, part B), 11577–11583 (2020), https://doi.org/10.1016/j.ceramint.2020.01.186

[13] M.I. Miranda-Lopez, E.A. Padilla-Zarate, M.B. Hernandez, L.A. Falcon-Franco, S. García-Villarreal, L.V. García-Quinonez, P. Zambrano-Robledo, A. Toxqui-Teran, and J.A. Aguilar-Martínez, Comparison between the use of Co_3O_4 or CoO on microstructure and electrical properties in a varistor system based on SnO_2, J. Alloys Compd. **824**, 153952 (2020), https://doi.org/10.1016/j.jallcom.2020.153952

[14] D. Liu, W. Wang, K. Cheng, Q. Xie, Y. Zhou, and H. Zhao, High voltage gradient and low leakage current SnO_2 varistor ceramics doped with Y_2O_3 and Nb_2O_5, Mater. Chem. Phys. **242**, 122526 (2020), https://doi.org/10.1016/j.matchemphys.2019.122526

[15] G. Hu, J. Zhu, H. Yang, and F. Wang, Effect of Cr_2O_3 addition on the microstructure and electrical properties of SnO_2-based varistor, J. Mater. Sci. **24**, 1735–1740 (2013), https://doi.org/10.1007/s10854-012-1007-z

[16] C.-M. Wang, J.-F. Wang, C.-L. Wang, H.-C. Chen, W.-B. Su, G.-Z. Zang, P. Qi, M.-L. Zhao, and B.-Q. Ming, Effects of barium on the nonlinear electrical characteristics and dielectric properties of SnO_2-based varistors, Chin. Phys. **13**(11), 1936–1940 (2004), https://doi.org/10.1088/1009-1963/13/11/031

[17] J.-F. Wang, H.-C. Chen, W.-B. Su, G.-Z. Zang, B. Wang, and R.-W. Gao, Effects of Sr on the microstructure and electrical properties of (Co, Ta)-doped SnO_2 varistors, J. Alloys Compd. **413**, 35–39 (2006), https://doi.org/10.1016/j.jallcom.2005.05.041

[18] S.R. Dhage, V. Ravi, and O.B. Yang, Varistor property of $SnO_2{\cdot}CoO{\cdot}Ta_2O_5$ ceramic modified by barium and strontium, J. Alloys Compd. **466**(1–2), 483–487 (2008), https://doi.org/10.1016/j.jallcom.2007.11.062

[19] P. Qi, J.-F. Wang, H.-C. Chen, W.-B. Su, W.-X. Wang, G.-Z. Zang, and C.-M. Wang, Nonlinear electrical properties of (Sr, Co, Nb)-doped SnO_2 varistors, Acta Phys. Sin. **52**(7), 1752–1755 (2003), https://doi.org/1000-3290/2003/52(07)/1752-04

[20] J.A. Aguilar-Martinez, A. Duran-Regules, A.B. Glot, M.B. Hernandez, M.I. Pech-Canul, and J. Castillo-Torres, Effect of CaO on the microstructure and non-ohmic properties of (Co, Sb)-doped SnO_2 varistors, Rev. Mex. Fis. **54**(1), 20–24 (2008).

[21] J.A. Aguilar-Martinez, E. Rodriguez, S. Garcia-Villarreal, L. Falcon-Franco, and M.B. Hernandez, Effect of Ca, Sr and Ba on the structure, morphology and electrical properties of (Co,Sb)-doped SnO_2 varistors, Mater. Chem. Phys. **153**, 180–186 (2015), https://doi.org/10.1016/j.matchemphys.2015.01.001

[22] M.I. Miranda-Lopez, A.E. Marino-Gamez, M.B. Hernandez, P.F. Martinez-Ortiz, L. Falcon-Franco, S. Garcia-Villarreal, L. Garcia-Ortiz, and J.A. Aguilar-Martinez, Influence of MCO_3 (M=Ca, Sr, Ba)-doping on the non-ohmic properties of the ceramic varistor system SnO_2–Co_3O_4–Cr_2O_3–Nb_2O_5, Ceram. Int. **47**(3), 4006–4011 (2021), https://doi.org/10.1016/j.ceramint.2020.09.267

[23] A.V. Gaponov and A.B. Glot, Varistor properties of SnO_2–Co_3O_4–Nb_2O_5–Cr_2O_3 ceramics baked at different temperatures, Visnyk Dnipro univ. **16**(2), 119–124 (2008) [in Ukrainian].

[24] M.I. Mendelson, Average grain size in polycrystalline ceramics, J. Am. Ceram. Soc. **52**(8), 443–446 (1969), https://doi.org/10.1111/J.1151-2916.1969.TB11975.X

[25] Z.-Y. Lu, Z. Chen, and J.-Q. Wu, SnO_2-based varistors capable of withstanding surge current, J. Ceram. Soc. Japan **117**(7), 851–855 (2009), https://doi.org/10.2109/jcersj2.117.851

[26] M.B. Hernandez, S. Garcia-Villareal, R.F. Cienfuegos-Pelaes, C. Gomez-Rodriguez, and J.A. Aguilar-Martinez, Structural, microstructure and electric properties of SnO_2-Sb_2O_5-Cr_2O_3 varistor ceramics doped with Co_2SnO_4 spinel phase previously synthesized, J. Alloys Compd. **699**, 738–744 (2017), https://doi.org/10.1016/j.jallcom.2016.12.419

[27] X. Fu, F. Jiang, R. Gao, and Z. Peng, Microstructure and nonohmic properties of SnO_2-Ta_2O_5-ZnO system doped with ZrO_2, Sci. World. J. **2014**, 754890 (2014), https://doi.org/10.1155/2014/754890

[28] H.S. Irion, E.C.F. de Souza, A.V.C. de Andrade, S.R.M. Antunes, and A.C. Antunes, Effect of Pr_6O_{11} doping in electrical and microstructural properties of SnO_2-based varistors, Acta Sci. Technol. **36**(2), 237–244 (2014), https://doi.org/10.4025/actascitechnol.v36i2.17995

[29] M.G. Masteghin and M.O. Orlandi, Grain-boundary resistance and nonlinear coefficient correlation for SnO_2-based varistors, Mater. Res. **19**(6), 1286–1291 (2016), https://doi.org/10.1590/1980-5373-MR-2016-0210

[30] Z.M. Jarzebski and J.P. Marton, Physical properties of SnO_2 materials. III. Optical properties, J. Electrochem. Soc. **123**(10), 333C–346C (1976), https://doi.org/10.1149/1.2132647

[31] A.V. Gaponov, Humidity sensors based on SnO_2–Co_3O_4–Nb_2O_5–Cr_2O_3 semiconductor varistor ceramics, Sens. Elektron. Mikrosist. Tehnol. **15**(3), 19–30 (2018), https://doi.org/10.18524/1815-7459.2018.3.142041

[32] A.V. Gaponov and O.V. Abramova, Electrical properties of tin oxide based varistors with PbO addition in humid air, Lith. J. Phys. **63**(1), 8–14 (2023), https://doi.org/10.3952/physics.2023.63.1.2

[33] A.B. Glot and Yu.A. Perepelitsa, The inhomogeneity of low voltage zinc oxide varistors, Electron. Technics. Ser. 5. Radioparts and Radiocomponents **2**(71), 35–37 (1988).

$CaCO_3$, $SrCO_3$ IR $BaCO_3$ PRIEMAIŠŲ POVEIKIS VARISTORINIŲ SnO_2 PAGRINDO KERAMIKŲ MIKROSTRUKTŪRAI IR ELEKTRINĖMS CHARAKTERISTIKOMS

A. Gaponov

Olesio Hončaro nacionalinis universitetas, Dnipras, Ukraina